International Journal of Fluid Machinery and Systems
Vol. 3, No. 2, April-June 2010

Original Paper

Computational Fluid Dynamics of Cavitating Flow in Mixed Flow Pump with Closed Type Impeller

Katsutoshi Kobayashi[1], Yoshimasa Chiba[2]

[1]Mechanical Mechanical Engineering Research Laboratory, Hitachi, Ltd.
832-2, Horiguchi, Hitachinaka, Ibaraki 312-0034, Japan, katsutoshi.kobayashi.kc@hitachi.com
[2]Hitachi Plant Technologies, Ltd.
603, Kandatsu-machi, Tsuchiura-shi, Ibaraki-ken, 300-0013 Japan, yoshimasa.chiba.zv@hitachi-pt.com

Abstract

LES(Large Eddy Simulation) with a cavitation model was performed to calculate an unsteady flow for a mixed flow pump with a closed type impeller. First, the comparison between the numerical and experimental results was done to evaluate a computational accuracy. Second, the torque acting on the blade was calculated by simulation to investigate how the cavitation caused the fluctuation of torque. The absolute pressure around the leading edge on the suction side of blade surface had positive impulsive peaks in both the numerical and experimental results. The simulation showed that those peaks were caused by the cavitaion which contracted and vanished around the leading edge. The absolute pressure was predicted by simulation with -10% error. The absolute pressure around the trailing edge on the suction side of blade surface had no impulsive peaks in both the numerical and experimental results, because the absolute pressure was 100 times higher than the saturated vapor pressure. The simulation results showed that the cavitation was generated around the throat, then contracted and finally vanished. The simulated pump had five throats and cavitation behaviors such as contraction and vanishing around five throats were different from each other. For instance, the cavitations around those five throats were not vanished at the same time. When the cavitation was contracted and finally vanished, the absolute pressure on the blade surface was increased. When the cavitation was contracted around the throat located on the pressure side of blade surface, the pressure became high on the pressure side of blade surface. It caused the 1.4 times higher impulsive peak in the torque than the averaged value. On the other hand, when the cavitation was contracted around the throat located on the suction side of blade surface, the pressure became high on the suction side of blade surface. It caused the 0.4 times lower impulsive peak in the torque than the averaged value. The cavitation around the throat caused the large fluctuation in torque acting on the blade.

Keywords: Cavitation, Numerical Simulation, Fluctuating Hydraulic Force, Pump, Blade

1. Introduction

In a pump, a large amount of stress occurs around the blade root due the hydraulic force acting on the blade. It is important to predict the stress numerically and evaluate a reliability of the strength for the pump structure. The hydraulic force is determined from the pressure distribution on the blade surface. The pressure difference between the pressure side and suction side of blade surface becomes the load bending the blade from the pressure side to suction side. The large amount of stress occurs around the blade root when the blade is bent by the hydraulic force.

A one-way coupled fluid and structure simulation was performed in a mixed flow pump with an open-type impeller[1]. The averaged stress was predicted by numerical simulation with a good computational accuracy. The largest stress occurred around the blade root at Q/Q_{bep}=70% flow rate in both the numerical and experimental results. The averaged stress was used to evaluate the low cycle fatigue of the structural strength of a pump. When the high cycle fatigue of the structural strength is evaluated, the fluctuating stress needs to be predicted. A two-way coupled fluid and structure simulation is needed to predict the fluctuating stress[2].

The hydraulic force acting on the blade is an unsteady one and this causes the stress fluctuation. One of the flow phenomena that cause this unsteady hydraulic force is the interaction between a rotating blade and a stator vane[3-6]. It causes the unsteady hydraulic forces in the blade passing frequency and its higher harmonic frequencies. On the other hand, the cavitation occurring inside the pump also causes the unsteady hydraulic force. It was shown in the experimental study that the stress fluctuation on the

Received February 23 2010; revised April 2 2010; accepted for publication April 4 2010: Review conducted by Prof. Tong-Seop Kim. (Paper number O10004K)
Corresponding author: Katsutoshi Kobayashi, Researcher, katsutoshi.kobayashi.kc@hitachi.com

blade surface was getting larger when the cavitation increased[7]. The cavitation causes the large unsteady hydraulic forces in the broadband frequencies.

The cavitation phenomena observed in hydraulic turbomachineries, such as axial flow pumps[8][9], inducer pump[10], and draft tube of Francis turbine[11], were analyzed by using a numerical simulation of the fluid dynamics. The cavitation performance or the region where the cavitation occurred was predicted by using numerical simulation. The cavitation in a turbopump inducer was simulated by LES[12]. It was found from this study that the cavitation vortex grew toward the upstream of the inducer blade when the NPSH was decreasing.

In this study, our objective is to analyze the cavitation phenomenon that causes the large unsteady hydraulic force acting on the blade. A mixed flow pump with the closed type impeller was simulated by LES with a cavitation model. The numerical results were used to show how the cavitation behaved inside the pump and caused the large unsteady hydraulic force on the blade.

2. Numerical Simulation Method

The mixed flow pump with the closed type impeller, which specific speed was 630, was simulated by the commercial software ANSYS CFX. The calculation domain is shown in Fig. 1. It includes a suction pipe, impeller and discharge pipe. The guide vanes that exist in the discharge pipe was neglected to reduce the computational grid number. The impeller has five blades and throat whose location is shown in Fig. 2. The inlet and outlet diameters of blade are 770 and 1270 (mm), respectively. An unstructured hexahedral mesh was made for the computational grid shown in Fig. 3. One blade was resolved by 334,723 grids and the total grid number was 2,194,278.

The constant total pressure corresponding to the NPSH was imposed on the inlet surface shown in Fig. 1. The constant mass flow rate was imposed on the outlet surface shown in Fig. 1. The simulated flow rate was Q/Q_{bep}=70%, and the rotating speed of impeller was 420 (min^{-1}). The specifications of pump are summarized in Table 1.

Table 1 Specifications of pump

Specific speed	630
Rotating speed	420 min^{-1}
Design flow rate (Q_{bep})	3.9 m^3/s
Head	12 m
Inlet diameter of blade	770 mm
Outlet diameter of blade	1270 mm

A homogeneous multiphase model was applied for the cavitation model[13]. The Rayleigh Plesset model, where the second order terms and the surface tension were neglected, was employed to describe the growth of a gas bubble. The saturated vapor pressure was 3171 (Pa). First, the steady flow was simulated by RANS with the cavitation model to make the initial flow condition for unsteady flow simulation. The $k-\omega$ based Shear-Stress-Transport (SST) model was applied for the RANS turbulence model [14]. Second, the unsteady flow was simulated by LES with the same cavitation model. The dynamic Smagorinsky model was applied for the LES turbulence model [15].

The advection term for the momentum equation was discretized by a second order upwind scheme in RANS and central difference scheme in LES[16]. The second order backward scheme was applied for the time marching method in LES[17].

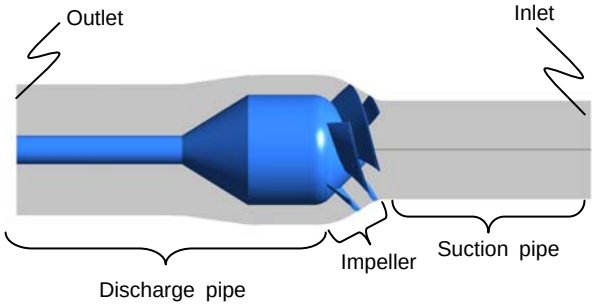

Fig. 1 Calculation domain used for simulation

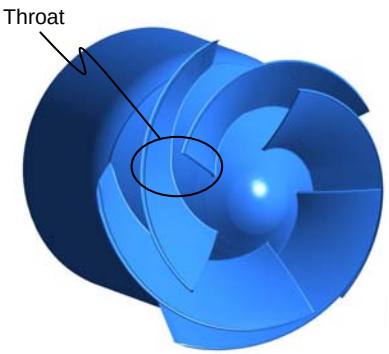

Fig. 2 Throat found in impeller

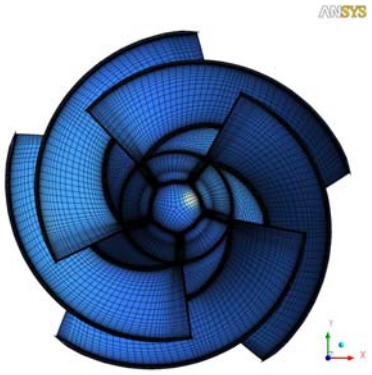

Fig. 3 Hexahedral mesh for computational grid

3. Experiment

The experiment was conducted in a recirculating water test loop with a suction tank. The pump was driven by a motor and the rotating speed was changed by an inverter. The flow rate was adjusted with a discharge valve and measured by using an electromagnetic flow meter. The total pressure was measured at two locations, the suction pipe and discharge pipe. The pump total head was calculated from the difference of total pressure between suction and discharge pipe. The pressure at the suction tank was controlled by a vacuum pump and a compressor for the experiment of cavitation performance.

The pressure on the suction side of blade surface was measured at two locations, SI and SO. SI was located near leading edge and SO was located near trailing edge. Fig. 4 shows a schematic diagram of pump used for the measurement of pressure. Two pressure sensors were installed at SI and SO and the wires of two sensors were picked up through the hollow shaft with a telemeter assembly.

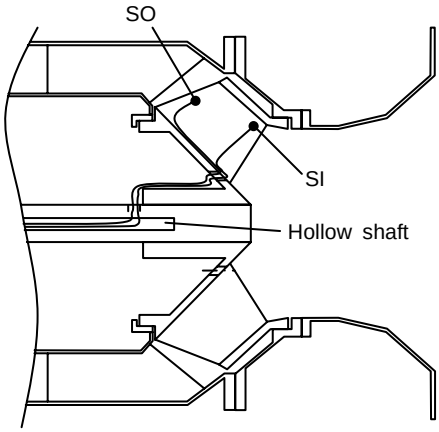

Fig. 4 Schematic diagram of pump used for the measurement of pressure

4. Validation for Numerical Results

To validate the cavitation model applied in ANSYS CFX, the cavitation performance for the pump was predicted by using RANS. The simulated flow rate was Q/Q_{bep}=70%. All simulations were carried out by parallel computation using 8 CPU of AMD Opteron 2218(Dual core). In RANS, all cases of simulation were continued until the pump total head converged to a constant value. The number of time steps needed for convergence was 200~600 steps and CPU time for 200 step was 7 hours in our hardware. The numerical result is compared to the experimental one in Fig. 5. The numerical total head was the difference in total pressure between the inlet and outlet of the blade. Both the numerical and experimental total heads were non-dimensionalized by the experimental total head when no cavitation occurred inside the pump. It could be predicted by numerical simulation that the total head decreased when the cavitation largely occurred in accordance with the decrease in NPSH. The cavitation model in ANSYS CFX could predict the cavitation performance with good accuracy.

The 2.5% head drop in the experimental result occurred at NPSH = 11 (m) in Q/Q_{bep}=70% flow rate and this NPSH condition was the minimum available NPSH in the operating condition. Therefore, the unsteady flow simulation by LES was performed at this NPSH = 11 (m) to predict the unsteady flow patterns more accurately than RANS. In LES, CPU time for one impeller revolution was 70 hours in our hardware. The absolute pressures were measured at SI and SO on the suction side of blade surface. The two points are shown in Fig. 6. The predicted absolute pressures at SI or SO are compared to experimental ones in Fig. 7 and Fig. 8, respectively. Both the numerical and experimental absolute pressures at SI had the positive impulsive peaks. The isosurface of 5% of the void fraction and the absolute pressure on the suction side of blade surface at two revolution times are shown in Fig.

9. Cavitation occurred around SI at 2.3774 revolution and the absolute pressure minimized at 3171 (Pa) which was the saturated vapor pressure. On the other hand, the cavitation vanished at 2.48584 revolution and the absolute pressure was higher than the saturated vapor pressure. That was why the absolute pressure at SI had the impulsive peaks. The positive impulsive peak was predicted by simulation with -10% accuracy. Cavitation did not occur around SO, because the absolute pressure was 100 times higher than the saturated vapor pressure. Therefore, the fluctuation of absolute pressure at SO was less than that at SI. It was concluded that the unsteady behavior of absolute pressure caused by cavitation was accurately predicted by our numerical simulation. The unsteady hydraulic force acting on the blade was discussed using the numerical results.

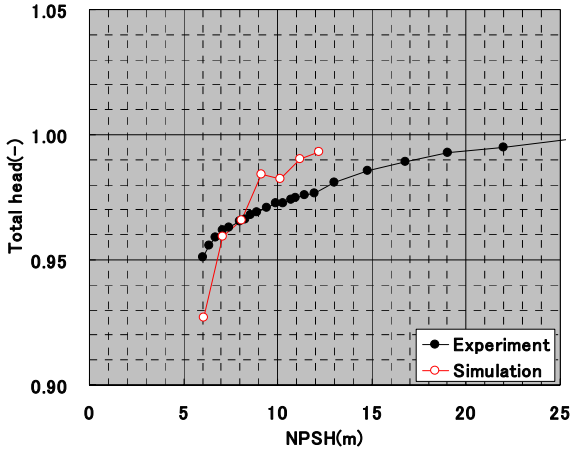

Fig. 5 Relation between NPSH and pump total head

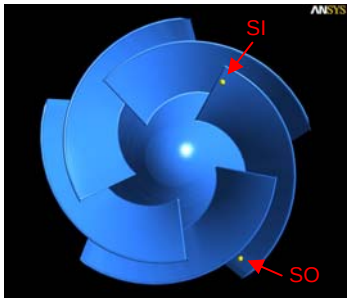

Fig. 6 Suction side pressure at two positions

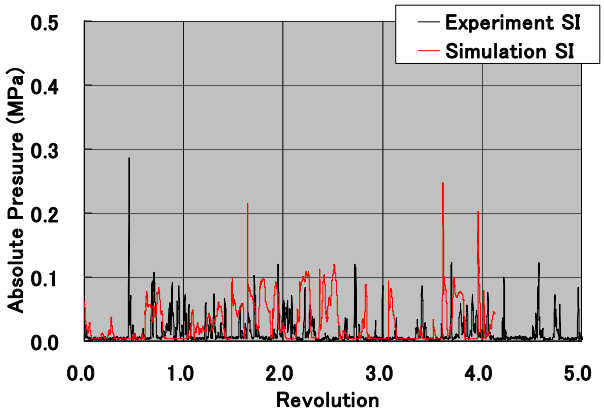

Fig. 7 Comparison of absolute pressure at SI

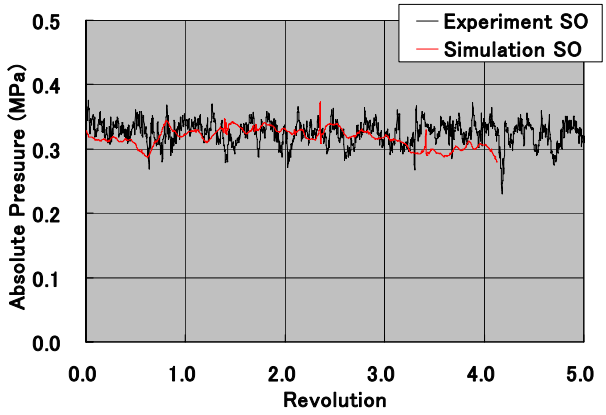

Fig. 8 Comparison of absolute pressure at SO

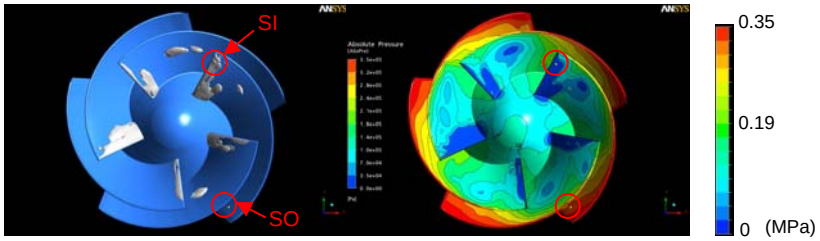

Revolution=2.3374

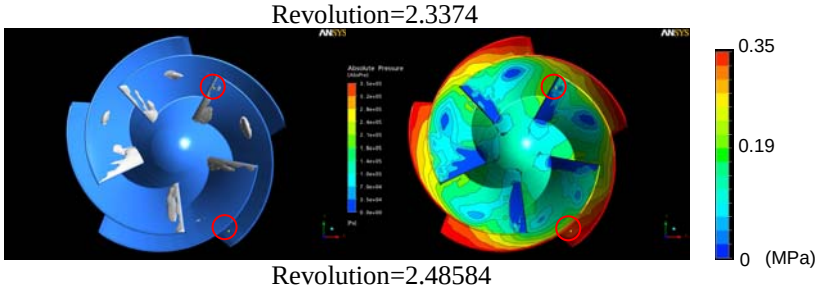

Revolution=2.48584

Fig. 9 5% of void fraction and absolute pressure at two revolutions

5. Unsteady Hydraulic Force

The unsteady hydraulic force acting on the blade was analyzed at NPSH = 11 (m), where 2.5% of head drop occurred at Q/Q_{bep}=70% flow rate. The torque was calculated on each of the five blades shown in Fig. 10. The time histories of the five torques are shown in Fig. 11. The total calculation time was about four revolution times and some impulsive peaks of torques indicated by circle are found after 2 revolution. Those impulsive peaks were caused by the unsteady cavitation phenomena. The flow state during the former 0-2 revolution times was the transitional stage from the initial flow calculated by RANS to the fully unsteady flow calculated by LES, therefore the later two revolution times were investigated. The torque of Blade3 had the 1.4 times higher impulsive peak than the averaged torque. And the torque of Blade4 had the 0.4 times lower impulsive peak than the averaged torque. Focus was put on the time histories of the three torques of Blade0, Blade3, and Blade4 between 2.0-2.5 revolution time, as shown in Fig. 12. Blade4 was located between Blade3 and Blade0. When Blade 4 had the positive impulse, Blade0 had the negative one. When Blade4 had the negative impulse, Blade3 had the positive one. The torque of Blade4 had the positive or negative impulsive peaks with the opposite phase against that of Blade0 or Blade3.

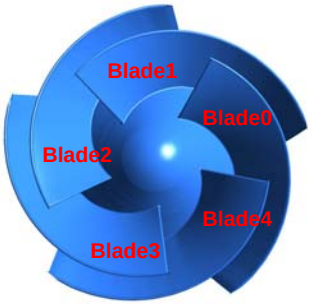

Fig. 10 Five blades where torques were calculated

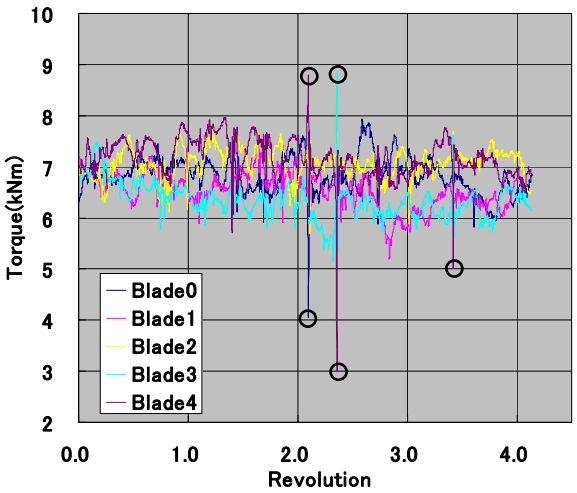

Fig. 11 Time histories of five torques

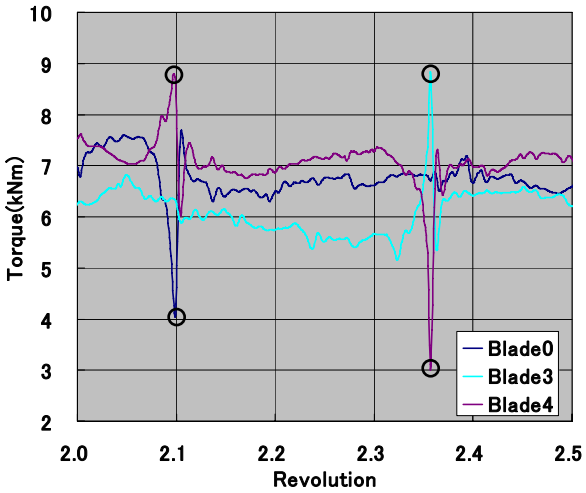

Fig. 12 Time histories of three torques between 2.0 and 2.5 revolution time

6. Analysis of Cavitation Behavior

It was found in the previous section that the time history of the torque had the positive or negative impulsive peaks. We investigated the cavitation behavior when the torque had the impulsive peak. Focus was put on the torques of Blade3 and Blade4 between 2.3-2.4 revolution time. In that revolution time, the torque of Blade3 had the positive impulsive peak and that of Blade4 had the negative impulsive one. The transient isosurface of 5% of the void fraction is shown in Fig. 13 when the torque of Blade4 had the negative impulsive peak. Six corresponding images are shown in Fig. 13. Cavitation occurred in two regions, one occurred around the leading edge on the suction side of blade surface, and the other occurred around the throat between Blade3 and Blade4. The magnitude of relative velocity and absolute pressure on the circular conical surface located at the mid-span of blade are shown in Fig. 14 and 15. The magnitude of the relative velocity was large around the throat and it caused the low absolute pressure. This was why cavitation occurred around the throat. It was found from Fig. 13 that the cavitation around the throat was contracting and finally vanished. When the cavitation was contracting, the torque of Blade4 was decreasing. The transient absolute pressure on the suction side of Blade4 surface is shown in Fig. 16 when the torque of Blade4 had the negative impulse. The absolute pressure was low around the throat where the cavitation occurred. When the cavitation was contracting, the absolute pressure around the throat was gradually increasing. The torque depends on the pressure difference between pressure side and suction side of blade surface. When the pressure on the suction side of blade surface becomes high, the torque becomes low. The increase in absolute pressure caused by the contraction of cavitaion around the throat provided the negative impulsive peak on the torque of Blade4.

The transient absolute pressure on the pressure side of Blade3 surface is shown in Fig. 17 when the torque of Blade3 had the positive impulsive peak. The revolution times of six images shown in Fig. 17 are the same as those of six images in Fig. 13 and Fig.16. Cavitation occurred not only around the throat but also around the leading edge on the pressure side of blade surface. The magnitude and vector of relative velocity are shown in Fig. 18 on the same circular conical surface as that in Fig. 14 and 15. The large magnitude of relative velocity occurred around the leading edge on the pressure side of Blade3 surface. This was why the absolute pressure was lowered and the cavitation occurred there. It was found from Fig. 17 that the cavitation around the leading edge was contracting in the same way as that around the throat. When the cavitation was contracting, the absolute pressure was increasing from downstream to upstream on the pressure side of Blade3 surface. This was why the torque of Blade3 increased and had the positive impulsive peak.

The torques of Blade3 and Blade4 were fluctuating in opposite phases. The positive and negative impulsive peaks of torque in Blade3 and Blade4 were observed at the same revolution time. And it was caused by the contraction of cavitation occurring around the throat between Blade3 and Blade4.

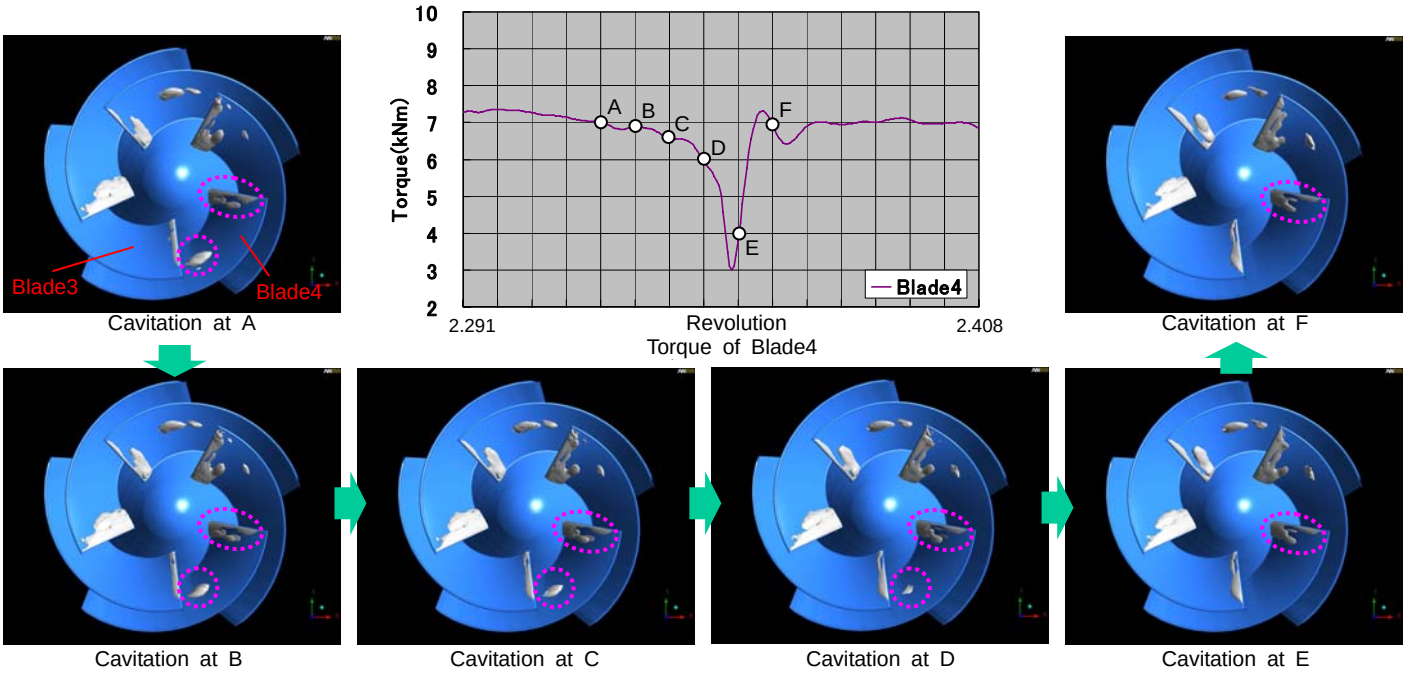

Fig. 13 Relation between cavitation behavior and torque of Blade4

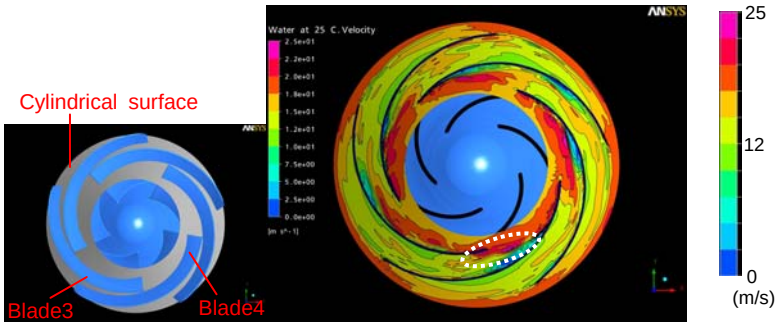

Fig. 14 Magnitude of relative velocity on cylindrical surface (Revolution is A in Fig. 13)

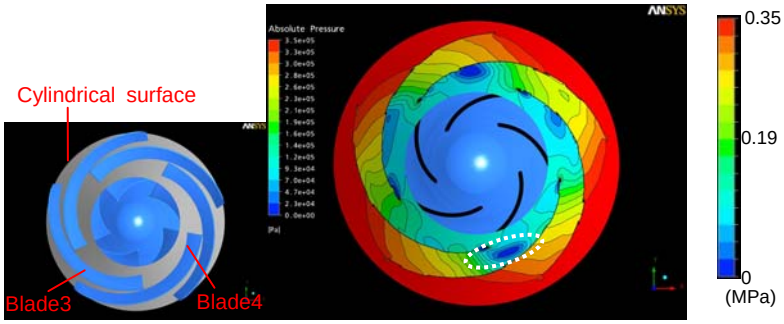

Fig. 15 Absolute pressure on cylindrical surface (Revolution is A in Fig. 13)

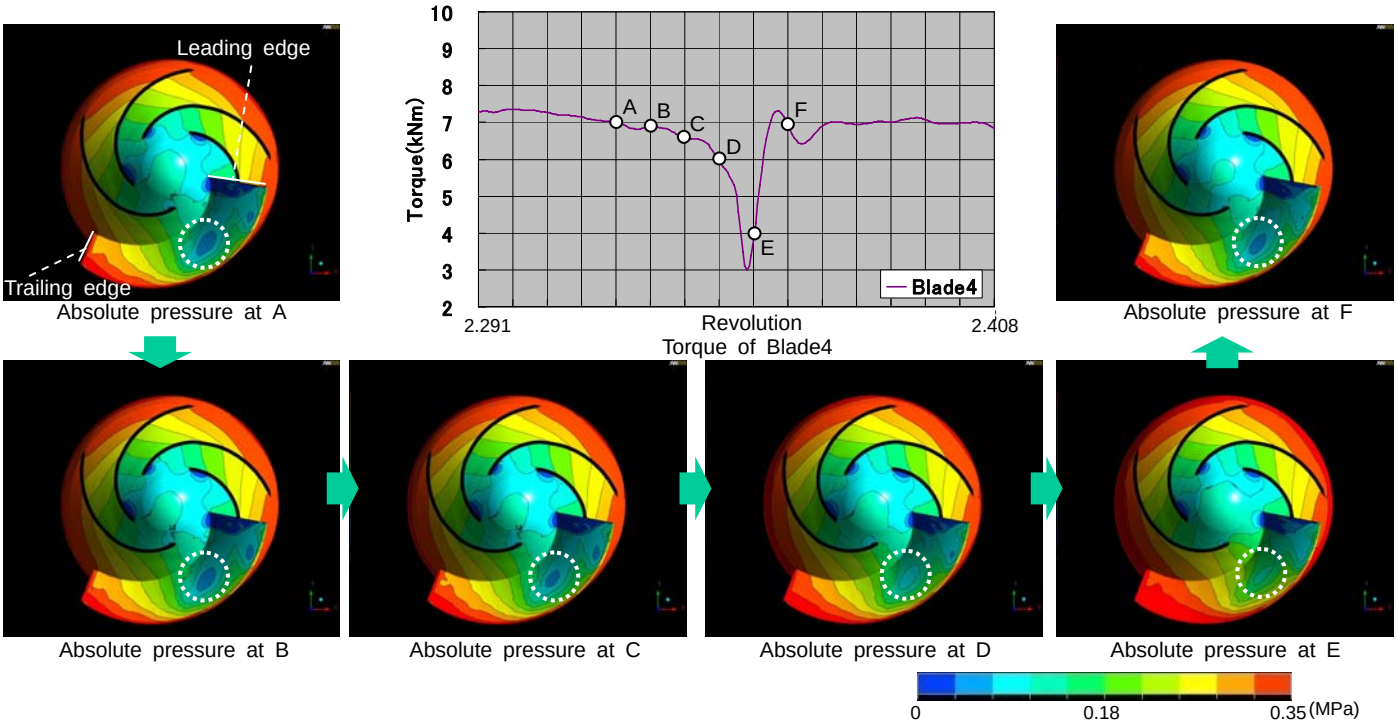

Fig. 16 Relation between absolute pressure and torque of Blade4

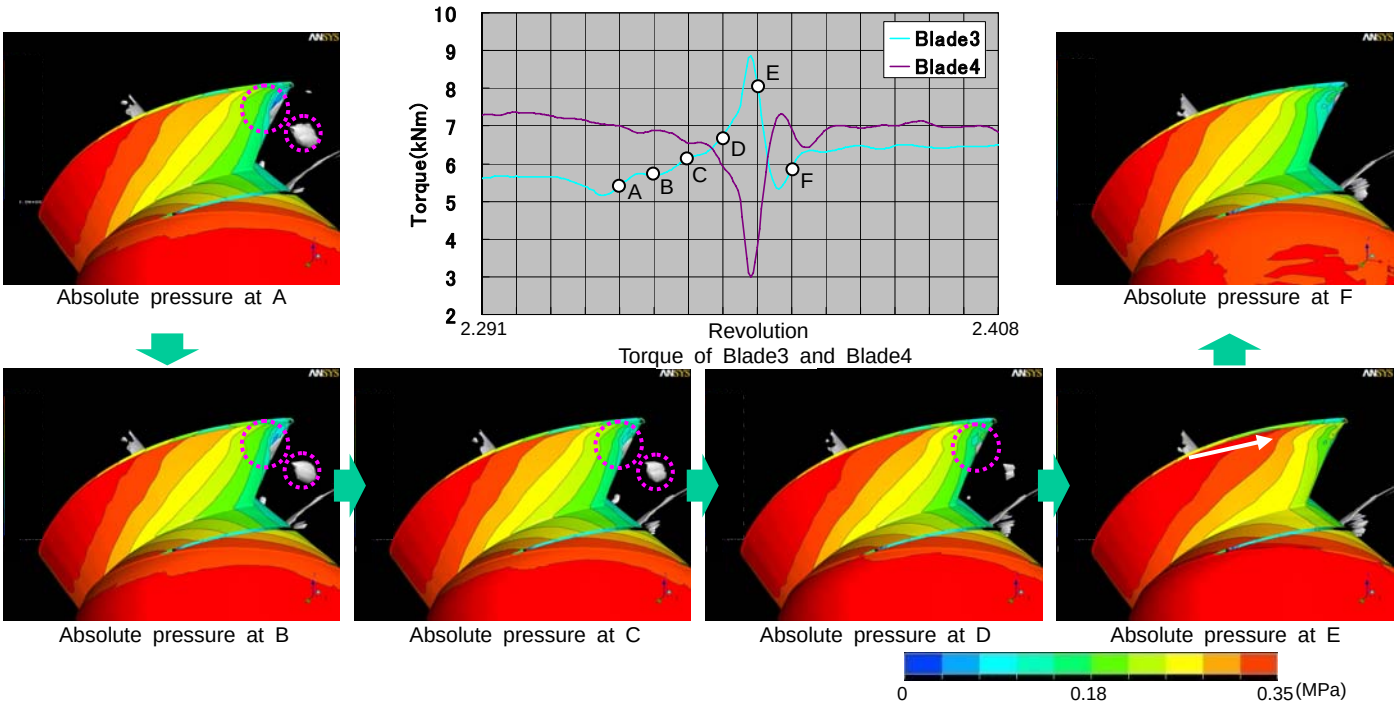

Fig. 17 Relation between absolute pressure and torque of Blade3

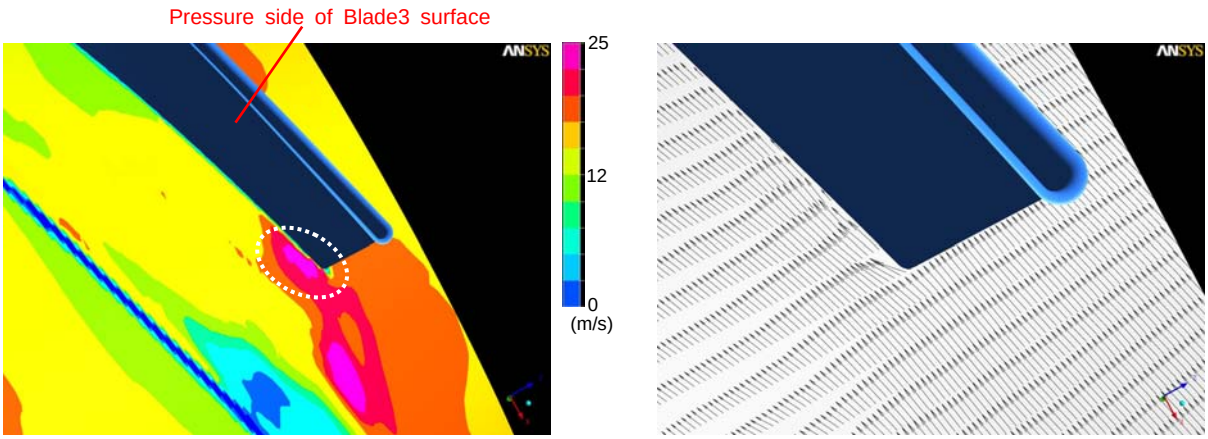

Fig. 18 Magnitude of relative velocity and relative velocity vector on cylindrical surface (Revolution is A in Fig. 17)

7. Conclusion

The unsteady flow simulation was performed by LES with cavitation model. The torque acting on the blade was calculated to evaluate the unsteady hydraulic force. The relationship between the torque fluctuation and the cavitation behavior was investigated and it was found that:

(1)Cavitation occurred around the leading edge on the suction side of blade surface. The absolute pressure around the leading edge on the suction side of blade surface had the positive impulsive peaks caused by cavitation. It was predicted by simulation with -10% accuracy. On the other hand, cavitation did not occur around the trailing edge on the suction side of blade surface, because the absolute pressure was 100 times higher than the saturated vapor pressure. The fluctuation in absolute pressure around the trailing edge on the suction side of blade surface was less than that around the leading edge.

(2)The torque acting on the blade had the impulsive peaks caused by cavitation. The maximum value of the positive impulsive peak in torque was 1.4 times higher than the averaged torque. The minimum value of the negative impulsive peak in torque was 0.4 times lower than the averaged torque.

(3) The simulation results showed that the cavitation was generated around the throat, then contracted and finally vanished. The simulated pump had five throats and cavitation behaviors such as contraction and vanishing around five throats were different from each other. For instance, the cavitations around those five throats were not vanished at the same time. When the cavitation

was contracted and finally vanished, the absolute pressure on the blade surface was increased. When the cavitation was contracted around the throat located on the pressure side of blade surface, the pressure became high on the pressure side of blade surface. It caused the 1.4 times higher impulsive peak in the torque than the averaged value. On the other hand, when the cavitation was contracted around the throat located on the suction side of blade surface, the pressure became high on the suction side of blade surface. It caused the 0.4 times lower impulsive peak in the torque than the averaged value. The cavitation around the throat caused the large fluctuation in torque acting on the blade.

In future work, a measurement of stress occurring on a blade root will be conducted and comparison between numerical torque and experimental stress will be performed to discuss a prediction method for stress by using numerical simulation.

Acknowledgments

We wish to thank Dr. Kouhei Tanaka of Hitachi, Ltd. for his helpful advice.

Nomenclature

Q	Pump discharge rate [m^3/s]	Q_{bep}	Discharge rate at best efficiency point [m^3/s]

References

[1] Kobayashi, K., Ono, S., Harada, I. and Chiba, Y., 2007, “Prediction of Stress on Pump Blade by One-Way Coupled Method of Fluid and Structure Simulations,” ASME International Mechanical Engineering Congress and Exposition, Seattle, Washington.
[2] Friedrich-Kari Benra, Hans Josef Dohmen and Bo Wan, 2006, “DETERMINATION OF PUMP IMPELLER DEFLECTIONS: COMPARISON OF FSI-SIMULATIONS TO MEASUREMENTS,” ASME Joint U.S. – European Fluids Engineering Summer Meeting, Miami, FL.
[3] Iino, T. and Kasai, K., 1985, “An Analysis of Unsteady Flow Induced by Interaction of Centrifugal Impeller and a Vaned Diffuser,” Trans. Jpn. Soc. Mech. Eng., (in Japanese), Vol. 51, No. 471, B, pp. 154-159.
[4] Arndt, N., Acosta, A. J., Brennen, C. E. and Caughey, T.K., 1989, “Rotor-Stator Interaction in a Diffuser Pump,” ASME J. of Turbomachinery, Vol. 111, pp. 213-221.
[5] Arndt, N., Acosta, A. J., Brennen, C. E. and Caughey, T.K., 1990, “Experimental Investigation of Rotor-Stator Interaction in a Centrifugal Pump with Several Vaned Diffusers,” ASME J. of Turbomachinery, Vol. 112, pp. 98-108.
[6] Guo, S., Okamoto, H. and Maruta, Y., 2006, “Measurement on the Fluid Forces Induced by Rotor-Stator Interaction in a Centrifugal Pump,” JSME International Journal, Series B, Vol. 49, No. 2, pp. 434-442.
[7] Yamaguchi, Y. and Ito, H., 1981, “Experimental Study for the fluctuation of Stress Caused on Runner Blade of High Head Pump,” Trans. Jpn. Soc. Mech. Eng., (in Japanese), Vol. 47, No. 413, B, pp. 95-104.
[8] Fukaya, M., Okamura, T., Tamura, Y. and Matsumoto, Y., 2003, “Prediction of Cavitation Performance of Axial Flow Pump by Using Numerical Cavitating Flow Simulation with Bubble Flow Model,” Fifth International Symposium on Cavitation, Osaka, Japan, November.
[9] Milan, S., Frantisek, M. and Pavel, S., 2001, “Numerical Investigation of Blade and Tip Clearance Geometry Influence on Tip Clearance and Tip Vortex Cavitations,” International Symposium on Experimental and Computational Aerothermodynamics of Internal Flows, Poland, Sept. 4-7.
[10] Okita, K. Matsumoto, Y. and Kamijo, K., 2003, “Numerical Analysis For Unsteady Cavitating Flow in a Pump Inducer,” Fifth International Symposium on Cavitation, Osaka, Japan, November 1-4.
[11] Charles C.S. Song, Xiangying Chen, Tani, K., Shinmei, K., Niikura, K. and Sato, J., 1999, “Simulation of Cavitating Flows in Francis Turbine and Draft Tube Under Off-design Conditions,” 3rd ASME/JSME Joint Fluids Engineering Conference, San Francisco, California.
[12] Nishimura, K., Kato, C., Yamade, Y., Yamanishi, N. and Tani, N., 2006, “Large Eddy Simulation of Unsteady Cavitating Flows in a Turbopump Inducer,” SEISAN KENKYU, (in Japanese), Vol. 58, No. 1, pp. 27-30.
[13] Help Navigator, ANSYS CFX, Release 11.0, ANSYS CFX-Solver Modeling Guide, Multiphase Flow Modeling, Interphase Mass Transfer, Cavitation Model.
[14] Help Navigator, ANSYS CFX, Release 11.0, ANSYS CFX-Solver Theory Guide, Turbulence and Wall Function Theory, Eddy Viscosity Turbulence Models, Two Equation Turbulence Models.
[15] Help Navigator, ANSYS CFX, Release 11.0, ANSYS CFX-Solver Modeling Guide, Turbulence and Near-Wall Modeling, Turbulence Models, The Large Eddy Simulation Model (LES).
[16] Help Navigator, ANSYS CFX, Release 11.0, ANSYS CFX-Solver Modeling Guide, Advice on Flow Modeling, Advection Scheme Selection.
[17] Help Navigator, ANSYS CFX, Release 11.0, ANSYS CFX-Solver Modeling Guide, Advice on Flow Modeling, Timestep Selection, Transient Timestep Control, Transient Scheme.